Int. J. Econ. Environ. Geol., Vol. 17, Issue 1, 2026, 35-44 doi: 10.46660/int.j.econ.environ.geol..v17i1.808
Journal home page: www.econ-environ-geol.org

ASSESSMENT OF CHANNEL MORPHOLOGY AND MIGRATION DYNAMICS OF THE JHELUM AND CHENAB RIVERS IN DISTRICT JHANG USING GEOSPATIAL TECHNIQUES

ATTIA-TUL-KAREEM, REHAN AHMAD PERVAIZ AND MIRZA NASEER AHMAD*
Abdus Salam School of Sciences, Nusrat Jahan College, Rabwah, Pakistan

Received: *20 February, 2026* ***Accepted:*** *25 March, 2026*

Abstract: In alluvial river systems, riverbank erosion, channel migration, and deposition processes play a crucial role in defining land use patterns and forming floodplain landscapes. Using District Jhang as the study area, this study examines spatiotemporal changes in channel morphology, riverbank erosion, and channel shifting along the Jhelum and Chenab rivers. Geoinformatics techniques were applied to analyze multi-temporal satellite imagery from 1992 to 2022 to assess morphological changes over 30 years. Channel planform characteristics, specifically sinuosity and centerline migration, were computed. The extent of floodplain transformation is determined by calculating erosion–accretion patterns. Significant morphological changes were shown in the river system. From 1992 to 2014, erosional processes dominated over depositional ones, resulting in a land loss of approximately 17,368.2 ha, compared to 4,728.01 ha of accretion. In contrast, the period from 2014 to 2022 indicates a shift toward sediment accumulation. During this time, erosion decreased to approximately 974.28 ha, while deposition significantly increased to about 7,659.98 ha. Spatial variations were observed in channel sinuosity: with the confluence zone showing a slight decrease in sinuosity, while increasing sinuosity in the upstream reaches of both rivers indicates enhanced meander development. The average migration rates of 36.59 m/year in the Upper Chenab reach, 17.66 m/year along the Jhelum River reach, and 38.18 m/year in the Lower Chenab reach disclosed a considerable lateral shifting in channel migration analysis. The results demonstrate the dynamic nature of the Jhelum–Chenab River system and its significant influence on floodplain development, and land stability in District Jhang. The Integration of Geographical Information Systems (GIS) and remote sensing technologies offers a robust approach for the long-term tracking of river morphological changes. It facilitates sustainable floodplain management and the development of erosion mitigation strategies.

Keywords: Channel morpho-dynamics, Geospatial techniques, Sinuosity index, Bankline shifting.

Introduction

Rivers continuously modify landscapes through erosion, sediment transport, and deposition, driving the evolution of channel and floodplain landforms (Okoroigwe *et al*., 2025). River–floodplain interactions, particularly during flood events, promote channel migration and planform adjustments, which are essential geomorphic processes but also pose risks to settlements, agricultural land, and infrastructure (Bibi *et al*., 2022; Debnath *et al*., 2017; Nagel *et al*., 2023; Zhang *et al*., 2020). In South Asia, monsoon-driven discharge and high sediment loads have intensified bank erosion, channel shifting, and floodplain transformation, resulting in substantial land loss and community displacement (Arefin *et al*., 2021; Dewan *et al*., 2017a). Similar channel instability has been reported in alluvial rivers worldwide, where hydro-climatic variability and sediment dynamics control lateral migration and planform change (Kumar *et al*., 2017). Within the Indus River system, the Jhelum and Chenab rivers are critical for agriculture, water supply, and hydropower, yet they have experienced significant planform adjustments and bank erosion, particularly during major floods (Fatima *et al*., 2025; Mahmood & Jia, 2016; Rahman *et al*., 2024). Recent studies further indicate that anthropogenic interventions and climate-driven hydro-climatic extremes are altering sediment and flow regimes, increasing channel instability and accelerating morphological change in these semi-arid alluvial rivers (Bibi *et al*., 2022; Debnath *et al*., 2017; Leenman *et al*., 2025).

Despite increasing recognition of river channel instability, systematic assessments of Bankline shifting and migration dynamics remain limited in many developing regions (Aishi & Fahim, 2024; Hasan *et al*., 2024). Bankline shifting, which reflects the spatial displacement of riverbanks in response to variations in discharge, sediment load, and flood frequency, is a key indicator of channel adjustment and instability (Debnath *et al*., 2017; Rahman *et al*., 2026). Climate change, coupled with monsoon flooding and upstream flow regulation, has altered channel curvature and sediment regimes, accelerating erosion, deposition, channel

Corresponding author e-mail: nmirza@njc.edu.pk

avulsion, and planform transformation (Baniya *et al*., 2023; Li *et al*., 2025; Sonowal *et al*., 2022). However, comprehensive reach-wise evaluations of migration rates and sinuosity changes over multi-decadal periods remain scarce, creating a critical knowledge gap that limits effective floodplain management, hazard mitigation, and sustainable land-use planning (Baniya *et al*., 2023; Rahman *et al*., 2026).

Recent advances in geoinformatics and multi-temporal satellite imagery have enabled effective monitoring of river morpho-dynamics, including channel migration, erosion–accretion dynamics, and planform changes (Arefin *et al*., 2021; Dewan *et al*., 2017b; Luqman *et al*., 2018). Techniques such as transect analysis are widely used to quantify lateral channel migration, while morphometric indices including sinuosity and braiding index help assess channel stability and planform transitions (Boota *et al*., 2021; Lovric & Tosic, 2016).

However, a significant research gap remains in the comparative assessment of neighboring river systems, particularly the Jhelum and Chenab rivers, where existing studies are largely confined to localized flood events and erosion hotspots (Hamid Ch *et al*., 2017). Moreover, no study has comprehensively integrated sinuosity variation, reach-wise migration rates, and directional migration trends within a standardized geospatial framework using consistent long-term datasets. Addressing this gap is essential for improving the understanding of long-term fluvial evolution and supporting sustainable river management and infrastructure planning in the region (Hazarika *et al*., 2015).

The objectives of this study are to evaluate the temporal variation in sinuosity of the Jhelum and Chenab rivers from 1992 to 2022, to analyze the spatial-temporal patterns of erosion and accretion during the periods 1992-2014 and 2014–2022, and to quantify reach-wise channel migration rates and directional shifts using multi-temporal satellite imagery and GIS-based techniques. By integrating morphometric analysis with geospatial methods, this study aims to improve the understanding of long-term river planform dynamics and to provide a robust scientific basis for sustainable floodplain management and hazard mitigation strategies.

Geology of Study Area

The total area of district Jhang is 6,351 square kilometers and consists of approximately 2.7 million population. Administratively, the district is divided into four tehsils: Jhang Tehsil, Ahmad Pur Sial Tehsil, Athara Hazari Tehsil, and Shorkot Tehsil. Jhang Sadar serves as the district headquarters. Economically, nearly 70% of the population is engaged in agriculture, making Jhang one of the major wheat-producing districts in Punjab. Other important crops cultivated in the area include sugarcane, rice, barley, tobacco, gram, and cotton.

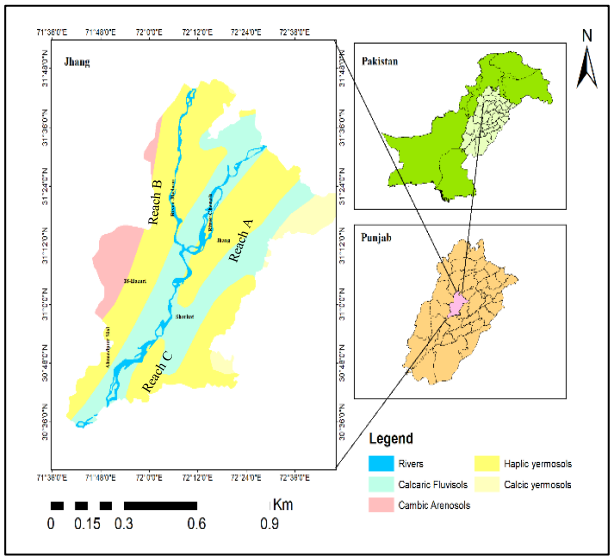

Fig. 1. Location map the study area.

District Jhang, located between 30°34′41″ N to 31°45′56″ N and 71°39′20″ E to 72°48′42″ E (Fig. 1). Jhang District lies within the active alluvial plains of the Indus Basin, and is predominantly composed of Quaternary deposits of sand, silt and clay laid down by the Chenab and Jhelum rivers. The district's geomorphology is characterized by continuous fluvial erosion, channel migration, and sediment deposition, particularly near the Chenab and Jhelum confluence at Trimmu. The floodplains contain fertile alluvial loam and silty soils, while the western Thal region is dominated by aeolian sandy deposits and dunes. Regular flooding and sediment replenishment have resulted in highly productive agricultural soils and a dynamic landscape that continues to evolve through ongoing depositional and erosional processes (Kondolf *et al*., 2014).

Materials and Methods

This study was conducted to assess river dynamics and morphological changes of the study area between 1992 and 2022.

The methodology was structured into three major objectives:
(1) assessment of changes in river sinuosity,
(2) quantification of erosion and accretion patterns, and
(3) analysis of channel migration rate and direction
The flow chart of methodology is shown in Fig.2.

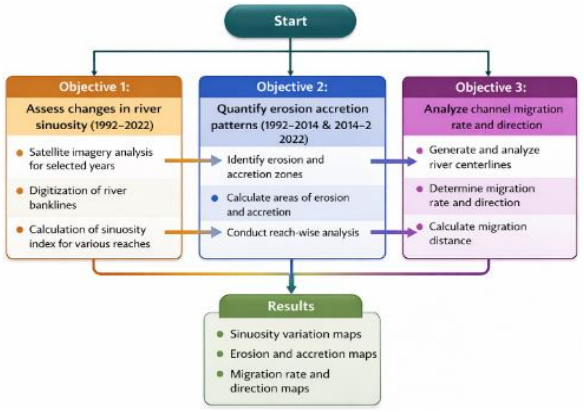

Fig. 2. Methodology flowchart.

Data Acquisition and Pre-processing

Multi-temporal satellite imagery from Landsat 5TM and Landsat 8OLI for the years 1992, 2014, and 2022 was used to analyze long-term channel dynamics. The study area falls within two adjacent Landsat path/rows (Row 38 and Row 39). Therefore, mosaicking was performed to merge the two scenes for each reference year to obtain a single, continuous image covering the entire study area. Following mosaicking, the images underwent geometric correction and were projected to a common coordinate system, this pre-processing ensured high spatial accuracy and reliable overlay analysis across the study periods. All analyses in this study were carried out using ArcGIS (version 10.8 ArcMap) and QGIS. The software was utilized for satellite image processing, supervised classification, identification of river centerlines, and determination of the mathematical values of bank erosion and accretion rates.

The evaluation of planform changes was done using ArcGIS 10.8 by manual digitization of riverbanks from the processed Landsat images. Channel boundaries for each reference year were delineated by digitization. Digitized Bankline helped in generating the River Centerline using standard GIS procedures. To enable detailed spatial analysis, based on geomorphological characteristics and channel behavior, the river was categorized into three reaches (Reach A, Reach B, and Reach C). These subdivisions facilitate in reach-wise comparison of morphological disparities. Valley length which is a straight-line distance between upstream and downstream points of each reach, and Channel length i.e. measured along the centerline, were computed. The equation used to calculate the sinuosity index (SI) is provided in Eq. 1, and the parameters of sinuosity ratio given in Table 1.

.

$$\text{Sinuosity Index (SI)} = \frac{\text{Channel Length}}{\text{Valley Length}} \qquad \text{Eq. 1}$$

Table 1. Parameters of sinuosity ratio.

Channel Pattern	Sinuosity Ratio (SR) Value
Straight	SR < 1.1
Sinuous	SR = 1.1 to 1.5
Meandering	SR > 1.5

Temporal variations were quantified by calculating the sinuosity index for each reach for the study years 1992, 2014, and 2022. The output consisted of thematic maps and tabulated data depicting spatial and temporal patterns of river sinuosity.

Quantification of Erosion and Accretion Patterns

River channel boundaries were extracted from multi-temporal satellite images using Supervised Image Classification with the Maximum Likelihood Classification (MLC) algorithm. This method accurately identified the water body class and produced a separate river shape file for each study year. The river centerline was then generated from the classified river polygons by extracting the midpoint between the left and right riverbanks. To determine riverbank erosion and accretion, an overlay intersection analysis was performed in ArcGIS between two consecutive river channel layers. This analysis identified the unchanged (overlapping) river area between the study years. Following the method of erosion and accretion areas were calculated using the Eq. 2 and Eq. 3.

$$\text{Amount of Erosion} = \text{Previous Year River Area} - \text{Unchanged Area} \qquad \text{Eq. 1}$$

$$\text{Amount of Accretion} = \text{Next Year River Area} - \text{Unchanged Area} \qquad \text{Eq. 2}$$

The annual rates of erosion and accretion (ha/year or km²/year) were calculated by dividing the total erosion and accretion areas by the corresponding time interval (Δt).

Analysis of Channel Migration Rate and Direction

Lateral channel migration was obtained by preparing river centerlines for all study years. Perpendicular transects were generated at regular intervals along the channel, and lateral displacement between centerlines of consecutive years (1992–2014, 2014–2022) was used to calculate migration distances. Spatial displacement relative to the flow direction was helpful in determining migration direction (left or right bank movement). The annual migration rate was computed by dividing the calculated migration distance by the time interval

Table 2. Erosion and accretion statistics of Jhelum and Chenab rivers in District Jhang.

Period	Erosion (ha)	Accretion (ha)	Erosion/Year (ha/year)	Accretion/ Year (ha/yr)	Net Change/ Year (ha/yr)	Total Changed Land (ha)	Remark
1992–2014	17,368.2	4,728.015	789.46	215.82	-574.55	22,096.2	Erosion
2014–2022	974.28	7,659.98	121.79	957.50	835.71	8,634.26	Net Accretion

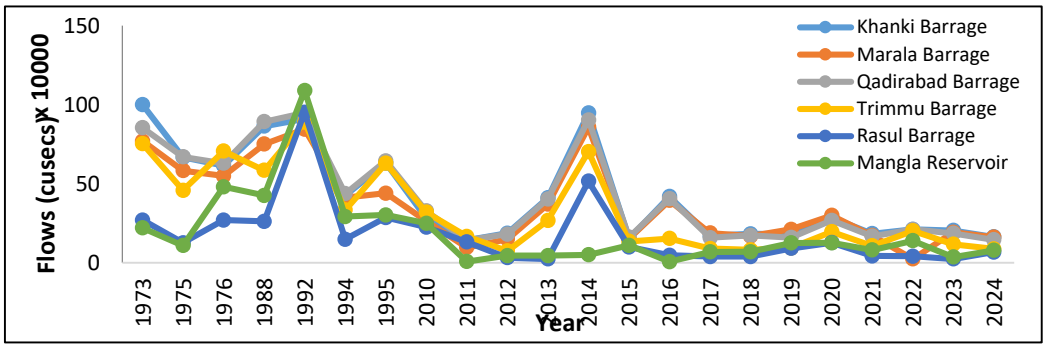

Fig. 3. Historical annual maximum peaks of different barrage locations at River Chenab and Jhelum (1973-2024) (Commission, 2024; Water et al., 2014).

between observations (m/year). It gives us a comparison between temporal intervals and river reaches. The product of this method comprises tabular form of migration distance, direction, and rate for each reach, and migration maps.

Results and Discussion

Changes in Channel Sinuosity (1992–2022)

The morphometric analysis of channel sinuosity for the Jhelum and Chenab rivers was conducted for 1992 and 2022 across three defined reaches (Reach A, Reach B, and Reach C). Measured sinuosity index (SI) values shows significant spatial-temporal variations, in channel planform geometry Table 2, Fig. 4).

Table 3. Morphological characteristics of Jhelum and Chenab rivers (1992-2022) in District Jhang.

River / Reach	Year	River Length (km)	Valley Length (km)	Sinuosity Index (SI)	River Type / Class
Reach B (Jhelum)	1992	66.32	61.05	1.08	Straight
	2022	68.50	60.33	1.13	Sinuous
Reach A (Chenab)	1992	50.34	46.31	1.08	Straight
	2022	52.08	45.07	1.15	Sinuous
Reach C (Confluence)	1992	69.94	61.49	1.13	Sinuous
	2022	67.07	62.53	1.07	Straight

Reach A of the Chenab River showed an increase in river length, from 50.34 km in 1992 to 52.08 km in 2022, while the valley length slightly decreased from 46.31 km to 45.07 km. The channel became more sinuous, with the sinuosity index rising from 1.08 to 1.15, indicating greater channel curvature and active lateral adjustments.

The Reach B of the Jhelum River experienced an increase in river length from 66.32 km in 1992 to 68.50 km in 2022 while the valley length slightly decreased from 61.05 km to 60.33 km. (Table 3). Over the same period, the sinuosity index increased from 1.08 to 1.13, reflecting a gradual shift from a relatively straight channel toward a more sinuous pattern.

Sinuosity index (SI) of the Jhelum-Chenab River system in District Jhang displays significant changes in planform geometry. The SI value approaching 1.15 within Reach A, occupying the upper Chenab area, and the SI value 1.13 for Reach B, having the Jhelum River area, showed a transition from "Straight" to "Sinuous" configuration Fig. 4 and Table 3. This transition depicts an active phase of lateral migration as the rivers adapt to runoff variations and sediment flux. According to Timár (2003), such rises in sinuosity are a primary mechanism for alluvial rivers to dissipate excess kinetic energy and approach a state of dynamic equilibrium.

In contrast, at the confluence Reach C shows, decreasing trend in sinuosity Table 3. The river length shortened from 69.94 km in 1992 to 67.07 km in 2022, while the valley length slightly increased from 61.49 km to 62.53 km. correspondingly, the sinuosity index dropped from 1.13 to 1.07, reflecting a shift toward a comparatively straighter channel. Overall, the findings show that the upstream reaches (Reach A and B) became more sinuous, whereas the confluence reach (Reach C) displayed a simpler, straighter channel form during the study period. The variations in morpho-dynamic processes across the study area are reflected by spatial variations.

On the other hand, for Reach C (Confluence), the SI value decreased from 1.13 to 1.07, presenting "channel straightening". This is a characteristic of high energy environments at river confluences. As noted by Hasan *et al*., (2024) confluence zones frequently face extreme hydraulic pressure during peak monsoonal discharges, which can trigger meandering, forcing the channel into a more linear and hydraulically efficient path. The geomorphic evolution of the river system between 1992 and 2022 displays two contrasting phases of channel dynamics.

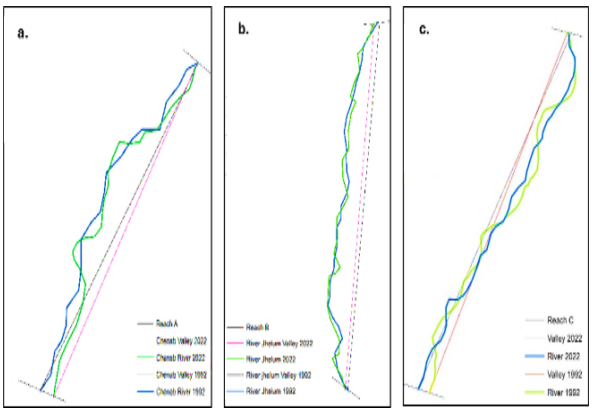

Fig. 4. (a) Sinuosity variation of Upper Chenab (Reach A) between 1992 and 2022 (b) Sinuosity variation of Jhelum River (Reach B) between 1992 and 2022 (c) Sinuosity variation of Lower Chenab (Reach C) between 1992 and 2022.

Erosion and Accretion Patterns

The spatial-temporal analysis of Bankline dynamics revealed significant variation in the erosion and accretion patterns between the two study periods from 1992-2014 and 2014-2022 (Fig. 5). The calculated statistics are presented in Table 2. Geomorphological activities peaked between 1992 and 2014, with erosion being the dominant process in the region. The area of eroded land reached 17,368.2 hectares, while in response, accretion helped only 4728.02 hectares to be restored. The Table 2 also shows that the accretion rate of 215.82 ha/year was far less than the erosion rate of 789.46 ha/year. This results in the mean yearly loss of 574.55 ha/year.

Collectively, the area eroded by these rivers reached 22,096.2 hectares, pointing to significant channel instability during this period. On the other hand, a reversal of trend is being observed from 2014 to 2022 (Fig. 5). Land loss through erosion was only 974.28 hectares, while the area gained through accretion was recorded 7659.98 hectares. The net annual erosion rate was 121.79 ha/year and accretion rate was of 957.50 ha/year. These results indicate an overall land gain of 835.71 hectares annually.

The geomorphic changes in the study area are closely linked to the river's hydrological regime, where discharge plays a key role in controlling bank stability. Between 1992 and 2014, the region experienced intense geomorphic activity due to several high-flood events, particularly in 1992, 1995 and 2014. Fig. 3. Discharge levels at Khanki Barrage, Marala Headworks, and Qadirabad Barrage reached very highpeaks, increasing hydraulic pressure on riverbanks and causing severe erosion. During this period, 17,368.2 hectares of land were lost, with an annual erosion rate of 789.46 ha/year, much higher than the accretion rate. In contrast, 2014–2022 shows a different pattern. The peak discharge declined after 2014, and generally remained below 400,000 cusecs (Fig. 3). Lower flow energy reduced erosion and promoted deposition. The erosion rate decreased to 121.79 ha/year, while accretion increased to 957.50 ha/year.

The results illustrate a marked transition from high-erosion environment (1992–2014) to accretion-dominated conditions (2014–2022). The three decades of study period faced significant morpho-dynamic adjustments in the river system.

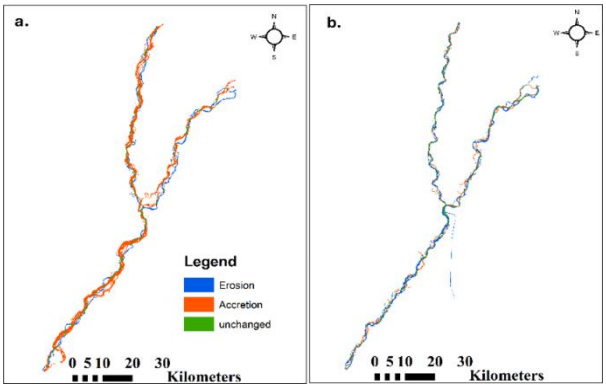

Fig. 5. (a) Erosion and Accretion Map of the Year 1992 and 2014. (b) Erosion and Accretion Map of the Year 2014 and 2022

Reach-wise erosion and accretion analysis (1992–2022): To further investigate the spatial patterns of geomorphic changes in the study area, erosion and accretion were analyzed on a reach-wise basis. The results indicate significant differences in land loss and gain among the three defined reaches Table 4. Reach A (Upper Chenab) shown in Table 4, experienced a total accretion of 2,577.81 hectares and total erosion of 3,315.58 hectares over the study period. The annual erosion rate of 110.52 ha/year suggests moderate channel activity compared to the downstream segments. Reach B (Jhelum River) shown in Table 4, experienced comparatively higher erosion, with a total land loss of 5,189.31 hectares and total accretion of 1,840.76

hectares. The calculated erosion rate of 172.98 ha/year indicated an increase in increased lateral instability and Bankline retreat within this reach.

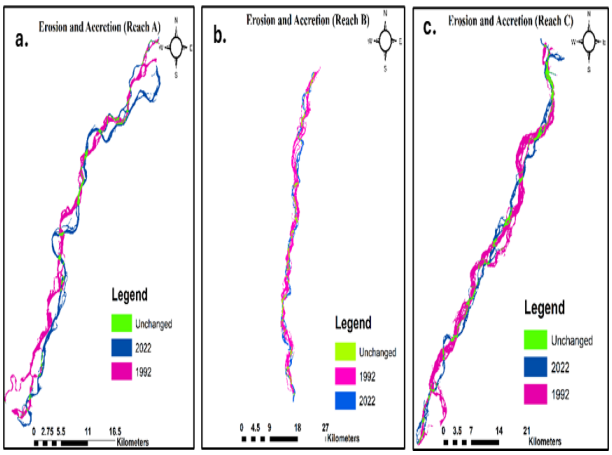

Fig. 6. (a) Net erosion and accretion (1992-2022) for Upper Chenab Reach. (b) Net erosion and accretion (1992-2022) for Jhelum River Reach (c) Reach A net erosion and accretion (1992-2022) for Lower Chenab River Reach.

Table 4. Erosion and accretion reach-wise in District Jhang.

Reach	Total Accretion (ha)	Total Erosion (ha)	Erosion Per Year (ha/yr.)
Reach A (Upper Chenab)	2,577.81	3,315.58	110.52
Reach B (Jhelum)	1,840.76	5,189.31	172.98
Reach C (Lower Chenab)	2,919.22	7,421.54	247.38

The highest geomorphological change was recorded in Reach C (Lower Chenab), shown in Table 4. Total accretion was 2,919.22 hectares, while the erosion was recorded at 7,421.54 hectares, and 247.38 ha/year of erosion rate made this segment the most vulnerable to erosional processes. The high rates of erosion propose enhanced morpho-dynamic processes in the downstream section. The total land area affected by erosion and accretion across all reaches calculated approximately 34,166.8 hectares. The spatial distribution of erosion indicates that downstream segments are more vulnerable to channel instability compared to upstream reaches.

Channel Migration Rate and Direction

The statistical analysis of the Jhelum River's centerline migration over 30 years discloses distinct planform dynamics across the three studied segments. Differences in migration rates and polygon frequency indicate varying levels of bank instability and complex meandering patterns.

Centerline migration analysis of Reach A (Upper Chenab) between 1992 and 2022 reveals noticeable lateral channel shifts. Seven migration segments were identified along Reach A, with the river centerline shift clearly illustrated in Table 6. The results indicate mixed directional movement. Four segments show westward migration toward the left bank, while three segments showed eastward movement toward the right bank. It suggets a prevailing lateral pressure on the western bank of Reach A.

Table 5. Average channel migration rate (m/year) in all three Resches

Segment	Total Polygons	Total Migration Distance (m)	Time Period (Years)	Average Migration Rate (m/year)
Segment A Upper	7	1097.68	30	36.59m/year
Segment C Lower Chenab	9	1145.27	30	38.18 m/year
Segment B Jhelum	18	529.65	30	17.66m/year

The alternating eastward and westward shifts reflect localized channel adjustments, likely associated with meander development and bank erosion processes. Overall, Reach A demonstrates dominant westward migration trends, indicating progressive channel instability and lateral shifting Fig. 7. Reach A, as shown in Table 5 exhibited a high migration rate of 36.59 m/year, despite having the fewest migration polygons (7) Table 6.

Table 6. Spatial attributes and directional movement of identified migration polygons (Sr. No. 1-7).

S. No.	Movement Direction	Side (L/R)
1	Eastward	Right
2	Westward	Left
3	Westward	Left
4	Westward	Left
5	Eastward	Right
6	Westward	Left
7	Eastward	Right

The centerline migration analysis for Reach B of the Jhelum River between 1992 and 2022 reveals significant lateral channel adjustments along the study reach Fig. 8, a total of eighteen migration segments were identified, representing spatial variability in river channel shifting over the study period. The results indicate alternating directional movement of the river channel, but migration happened almost equally towards both banks. Out of the eighteen analyzed segments, nine segments (segments 1, 3, 5, 7, 9, 11, 13, 15, and 17) exhibited westward migration toward the left bank, whereas the remaining

nine segments (segments 2, 4, 6, 8, 10, 12, 14, 16 and 18) showed eastward migration toward the right bank Table 7. This balanced directional distribution shows continuous lateral oscillation rather than erosion on one side. The repeated alternations reflect active meandering behavior and localized erosion–deposition processes in Reach B.

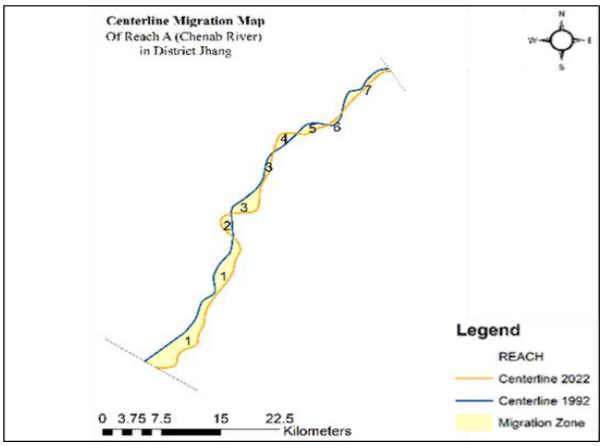

Fig. 7. Centerline migration of reach A (Chenab River) from 1992 to 2022.

Table 7. Spatial attributes and directional movement of identified migration polygons (Sr. No. 1-18).

Sr. No.	Movement Direction	Side (L/R)	Sr. No.	Movement Direction	Side (L/R)
1	Westward	Left	10	Eastward	Right
2	Eastward	Right	11	Westward	Left
3	Westward	Left	12	Eastward	Right
4	Eastward	Right	13	Westward	Left
5	Westward	Left	14	Eastward	Right
6	Eastward	Right	15	Westward	Left
7	Westward	Left	16	Eastward	Right
8	Eastward	Right	17	Westward	Left
9	Westward	Left	18	Eastward	Right

Centerline migration analysis for Reach C (Lower Chenab River) between 1992 and 2022 reveals noticeable lateral channel adjustments within the study area, Reach C shows a stabilized and actively meandering river section, specifically controlled by downstream hydraulic adjustments near the confluence zone. This region illustrated the highest degree of lateral instability, with a total migration distance of 1,145.27 m, in Table 5. The corresponding average migration rate of 38.18 m/year suggests intense bank erosion and rapid channel shifting in this reach.

A total of nine migration segments were identified, indicating spatial variation in the shifting behavior of the river centerline during the study period. This Table 8 also shows alternating directional migration of the river channel. Five segments exhibited westward migration toward the left bank, while four segments showed eastward migration toward the right bank. The results suggest relatively greater lateral pressure and erosion activity along the left bank of the Lower Chenab River. Meander development and localized bank erosion and deposition processes can be indicated by alternating shifts.

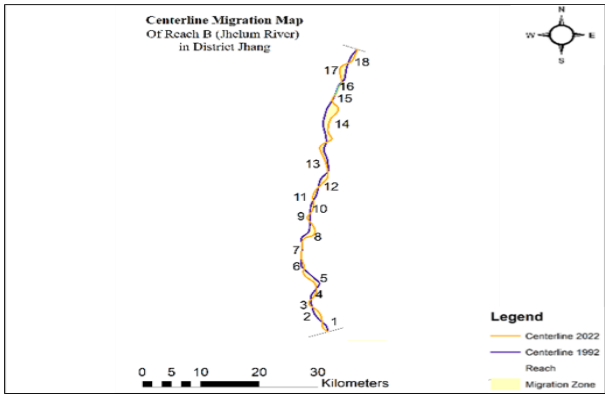

Fig. 8. Centerline migration of Reach B (Jhelum River) from 1992 to 2022.

Table 8. Spatial attributes and directional movement of identified migration polygons (Sr. No. 1-9).

Sr. No.	Movement Direction	Side (L/R)	Sr. No.	Movement Direction	Side (L/R)
1	Eastward	Right	6	Westward	Left
2	Westward	Left	7	Eastward	Right
3	Westward	Left	8	Westward	Left
4	Westward	Left	9	Eastward	Right
5	Eastward	Right			

Reach C shows a stabilized and actively meandering river section, specifically controlled by downstream hydraulic adjustments near the confluence zone. This region illustrated the highest degree of lateral instability, with a total migration distance of 1,145.27 m, in Table 5.The corresponding average migration rate of 38.18 m/year suggests intense bank erosion and rapid channel shifting in this reach.

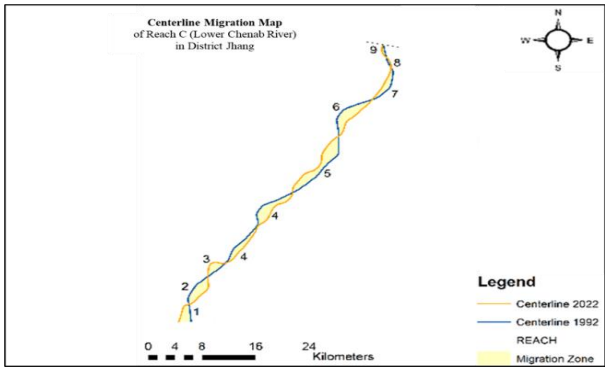

Fig. 9. Centerline migration of reach C (Chenab River) from 1992 t 2022.

Table 9. Migration direction and length of Jhelum and Chenab rivers in District Jhang.

Transect ID	Length (km)	Transect ID	Length (km)	Transect ID	Length (km)	Transect ID	Length (km)
1	1.16	21	0.56	11	0.54	31	0.23
2	0.2	22	1.02	12	0.18	32	0.9
3	0.01	23	0.55	13	0.02	33	0.56
4	0.72	24	0.82	14	1.9	34	0.99
5	1.6	25	0.48	15	1.41	35	1.37
6	1.02	26	0.01	16	0.44	36	0.09
7	1.41	27	0.89	17	1.85	37	0.81
8	1.24	28	0.08	18	0.2	38	0.56
9	0.12	29	0.69	19	0.6	39	0.9
10	1.89	30	0.31	20	0.97	40	0.1

The maximum velocity 38.18 m/year of migration rate in Reach C, shows intense geomorphic mobility. 1098.68m of westward migration in Reach A, and 18 migration polygons of Reach B prove that the system is facing continuous planform evolution. These lateral shifts are supported by the work of S onowal *et al*. (2022), who emphasize that channel migration is not solely a natural response, but is strongly controlled by bank material composition and sediment flux.

Spatiotemporal Channel Migration Analysis in District Jhang

spatiotemporal analysis of channel migration focusing on the Chenab and Jhelum Rivers, shows significant planimetric adjustments occurred during the study period (1992–2022). Forty transects were established across the study area to measure lateral channel dynamics for assessment of directional variations and migration distance Fig. 10.

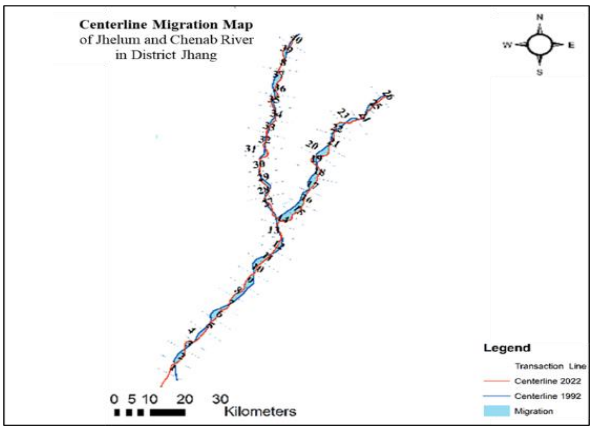

Fig. 10. Direction of overall river migration of 1992 and 2022.

Quantitative analysis exhibits highly dynamic fluvial behavior in this region, characterized by continuous lateral adjustments. Migration distances show spatial variability, reflecting the complex hydro-geomorphological conditions governing channel evolution in the Jhang region. Approximately 0.74 km was the average channel migration, indicating medium to high lateral instability of river channels. Maximum channel displacement recorded at transect number 14. Whereas the minimum channel shift was 0.01 km at transect 3 and transect 26. Sediment transport dynamics, flow energy distribution, bank material resistance, and anthropogenic interventions in river embankments were main reasons for variations in migrations patterns (Table 9). The channel behavior assessment from 2014 to 2022 exhibits a significant shift from erosion-dominated to accretion-dominated environments (Table 2). The net accretion was approximately 835.71 ha yr^{-1}.This transition indicates variations in hydraulic energy conditions and sediment balance. This impacted channel stabilization during 2014-2022.

Directional analysis shows that channel migration occurred through both eastward and westward shifts, indicating meandering river dominance rather than uniform lateral displacement. Reach-wise analysis shows spatial variations in channel instability. Geomorphologically, Reach C is highly vulnerable, with erosion reaching 7421.54 ha, and the annual rate was 247.38 ha yr^{-1}. These results indicate the alarming situation in the southern part of the district, which is vulnerable to substantial land loss and channel adjustment. Whereas, Reach B covering the Jhelum River, westward migration patterns are showing sustained lateral pressure towards the left bank. The northern part of study presented alternating migration trends, showing meandering structure and erosion deposition processes.

Conclusion

Remote sensing and Geographic Information System (GIS) techniques provide an effective and reliable approach for analyzing long-term river morphological dynamics, particularly for assessing bank erosion, accretion processes, and channel migration. The results revealed significant variations in erosion and accretion patterns over the study period. During the first phase

(1992–2014), erosion was the dominant geomorphic process, with approximately 17,368.2 ha of land loss due to bank erosion, while accretion accounted for only 4,728.01 ha. This resulted in a substantial net annual land loss of approximately 574.55 ha/year, indicating intense channel instability and active lateral migration during this period. However, a clear shift in geomorphic dynamics was observed in the later phase (2014–2022), when erosion decreased significantly to 974.28 ha, and accretion increased to 7,659.98 ha. Consequently, the river system experienced a positive net annual land gain of approximately 835.71 ha/year, suggesting a transition toward depositional dominance and relative channel stabilization. The analysis of channel sinuosity further highlighted the morphological evolution of the river system.

References

Agriculture Department, Government of the Punjab. (2014). *Punjab agriculture profile*. Government of the Punjab, 1-60.

Arefin, R., Meshram, S.G. and Seker, D.Z. (2021). River channel migration and land-use/land-cover change for Padma River at Bangladesh: a RS- and GIS-based approach. *Int. J. Environ. Sci. Technol*., **18**(10): 3109-3126.

Baniya, S., Deshar, R., Chauhan, R. and Thakuri, S. (2023). Assessment of channel migration of Koshi River in Nepal using remote sensing and GIS. *Environmental Challenges*, **11**(9): 100692.

Bibi, S., Nadeem, B., Bux, R. and Khan, S. (2022). Impact of flood disaster on the people's livelihood and adaptation to its effects in the Chenab riverine area, Multan District, Punjab, Pakistan (1992-2015). *J. Himal. Earth Sci*., **34**(1): 195-198.

Boota, M.W., Yan, C., Idrees, M.B., Li, Z., Soomro, S.E.H., Dou, M., Zohaib, M. and Yousaf, A. (2021). Assessment of the morphological trends and sediment dynamics in the Indus river, Pakistan. ***J.** Water Clim. Change***, 12**(7): 3082–3098.

Board of Revenue, Government of the Punjab. (2021). *The gazetteer of the Jhang district 2021*. District Administration Jhang.

Debnath, J., Das (Pan), N., Ahmed, I. and Bhowmik, M. (2017). Channel migration and its impact on land use/land cover using RS and GIS: A study on Khowai River of Tripura, North-East India. *Egypt. J. Remote Sens. Space Sci*., **20**(2): 197-210.

Dewan, A., Corner, R., Saleem, A., Rahman, M.M., Haider, M.R., Rahman, M.M. and Sarker, M.H. (2017a). Assessing channel changes of the Ganges-Padma River system in Bangladesh using Landsat and hydrological data. *Geomorph*., **276**: 257-279.

Dewan, A., Corner, R., Saleem, A., Rahman, M.M., Haider, M.R., Rahman, M.M. and Sarker, M.H. (2017b). Assessing channel changes of the Ganges-Padma River system in Bangladesh using Landsat and hydrological data. *Geomorph.*, **276**: 257-279.

District Administration Jhang, Government of the Punjab. (n.d.). *Geography*. Retrieved February 28, 2026.

District Disaster Management Authority Jhang. (2011). *District disaster risk management plan: Jhang*. National Disaster Management Authority; Provincial Disaster Management Authority Punjab. NDMA Library.

Fatima, R., Atif, S., Fort, M. and Azmat, M. (2025). Channel morphology of the Indus, and the growing risk of floods related damages in the Indus River basin. *Natural Hazards*, **121**(13): 15789-15821.

Federal Flood Commission. (2024). *Annual flood report 2024*. Ministry of Water Resources, Government of Pakistan. Federal Flood Commission.

Hamid Ch, M., Ashraf, M., Hamid, Q., Sarwar, S.M. and Saqib, Z.A. (2017). Geospatial techniques for assessment of bank erosion and accretion in the Marala Alexandria reach of the River Chenab, Pakistan. *Sains Malaysiana*, **46**(3): 413-420.

Hasan, I., Dey, J., Munna, M.M.R., Preya, A., Nisanur, T.B., Memy, M.J. and Zeba, M.Z.S. (2024). Morphological changes of river bank erosion and channel shifting assessment on Arial Khan River of Bangladesh using Landsat satellite time series images. *Prog. Disaster Sci*, **24**: Article 100381.

Hazarika, N., Das, A.K. and Borah, S.B. (2015). Assessing land-use changes driven by river dynamics in chronically flood affected Upper Brahmaputra plains, India, using RS-GIS techniques. *Egypt. J. Remote Sens. Space Sci*., **18**(1): 107-118.

Kondolf, G.M., Gao, Y., Annandale, G.W., Morris, G.L., Jiang, E., Zhang, J., Cao, Y., Carling, P., Fu, K., Guo, Q., Hotchkiss, R., Peteuil, C., Sumi, T., Wang, H., Wang, Z., Wei, Z., Wu, B., Wu, C. and Yang, C.T. (2014). Sustainable sediment management in reservoirs and regulated rivers: Experiences from five continents. *Earth's Future*, **2**(5): 256-280.

Kumar, P., Rahman, A. and Anika Yunus, D. (2017). Analysis on River Bank Erosion-Accretion and Bar Dynamics Using Multi-Temporal Satellite Images. *Am. J. Water Resour.*, **5**(4): 132-141.

Leenman, A., Greenberg, E., Moulds, S., Wortmann, M., Slater, L. and Ganti, V. (2025). Accelerated River mobility linked to water discharge variability. *Geophys. Res. Lett.*, **52**(2): e2024GL112899.

Li, C., Wang, Z., Lu, Y., Zhu, L., Dong, B., and Wei, X. (2025). Effects of River migration and water-sediment regulation scheme on total nitrogen transport in the yellow River Estuary. *Sustainability*, **17**(20): 9145.

Local Government and Community Development Department, Government of the Punjab. (n.d.). *District Jhang*. Retrieved February 28, 2026.

Lovric, N., and Tosic, R. (2016). Assessment of Bank Erosion, Accretion and Channel Shifting Using Remote Sensing and GIS: Case Study - Lower Course of the Bosna River. *Quaest. Geogr.,* **35**(1): 81-92.

Luqman, M., Shah, U. U. H., Khan, S., and Akmal, F. (2018). River channel dynamics detection using remote sensing and GIS technologies: A case study of River Chenab in Indo-Pak region. *In*: 2017 5th International Conference on Aerospace Science and Engineering (ICASE), IEEE, 1-5.

Mahmood, R., and Jia, S. (2016). Assessment of Impacts of Climate Change on the Water Resources of the Transboundary Jhelum River Basin of Pakistan and India. *Water,* **8**(6): 1-19.

Nagel, G.W., Darby, S.E., and Leyland, J. (2023). The use of satellite remote sensing for exploring river meander migration. *Earth-Sci. Rev.,* **247**(March): 104607.

Okoroigwe, N. I., Nkemdirim, V. U., and Ojo, O. A. (2025). Fluvial and geomorphological analysis of river dynamics and impact. *Int. J. Sci. Res. Arch.*, **14**(3): 290-300.

Pakistan Bureau of Statistics. (2023). *7th population and housing census 2023: The digital census*. Ministry of Planning Development and Special Initiatives, Government of Pakistan.

Rehan, W. (n.d.). *Punjab-Jhang*. Pakistan Almanac. Retrieved February 28, 2026.

Rahman, K.U., Shang, S., Balkhair, K.S., Gabriel, H.F., Jadoon, K.Z., and Zaman, K. (2024). Catchment-scale assessment of drought impact on environmental flow in the Indus Basin, Pakistan. *Nat. Hazards Earth Syst. Sci*., **24**(6): 2191-2214.

Rahman, M.S., Habib, S.M.A., Ashik, M.J., Sharif, M. and Sharifee, M.N.H. (2026). Bankline Shifting and Sand Bar Dynamics of the Teesta River Using Multi-Temporal Satellite Images. *Dhaka Univ. J. Earth Environ. Sci*., **14**(2): 33-49.

Sonowal, G., Thakuriah, G., and Hazarika, S. (2022). Role of Channel Migration and Influencing Hydro-Geomorphic Attributes in Dibru River Basin Using Remote Sensing and GIS. *Nat. Environ. Pollut. Technol*., **21**(5): 2035-2054.

Timár, G. (2003). Controls on channel sinuosity changes: A case study of the Tisza River, the Great Hungarian Plain. *Quat. Sci. Rev.,* **22**(20): 2199-2207.

Water, M.O.F., Of, O., Chief, T.H.E., Advisor, E., Federal, C. and Commission, F. (2014). Government of Pakistan Ministry of Water and Power Annual Flood Report 2014.

Zhang, W., Hu, B., and Brown, G.S. (2020). Automatic Surface Water Mapping Using Polarimetric. *Water*, **12**(3): 872.